ROSE COTTAGE, TYLER'S GREEN, Penn, Buckinghamshire: Archaeomagnetic Dating Report 2004

Paul Linford

Summary

During excavations in advance of redevelopment at Rose Cottage, Tyler's Green near Penn in Buckinghamshire, a series of medieval and post-medieval tile kilns were discovered. Finds at the site included a number of decorated medieval floor tiles of a type characteristic of the Penn area in the late medieval period. Archaeomagnetic analysis of two kilns from the site suggests that both were last used in a later period, one in the fifteenth century and the other in the sixteenth or seventeenth century. However, there was evidence that magnetic distortion might have affected the earlier date, whilst individual magnetisation direction measurements for the later date were surprisingly inconsistent for such a well fired feature.

ROSE COTTAGE, TYLER'S GREEN, Penn, Buckinghamshire:
Archaeomagnetic Dating Report 2004

Introduction

During excavations by Archaeological Services and Consultancy Ltd. (ASC) in advance of redevelopment at Rose Cottage, Tyler's Green near Penn in Buckinghamshire (NGR: SU 907 939, Longitude 0.7°W, Latitude 51.6°N), a series of medieval and post-medieval tile kilns were discovered (Fell, 2001). Finds at the site included a number of decorated medieval floor tiles. The floor tile industry at Penn in the late medieval period was of considerable importance with its product being used at the royal manors at Sheen and the Tower of London in the 1380s. Hence, the discovery was deemed to be of regional or possibly national significance and, as a result, the English Heritage Inspector of Ancient Monuments for Buckinghamshire, Christopher Welch, requested that the Centre for Archaeology (C*f*A) assist with archaeomagnetic analysis. Two kilns were thus sampled by the Museum of London Archaeology Service (MoLAS) Geomatics Team on behalf of the C*f*A during August 2003. The author performed all subsequent measurement and analysis.

Figure 1: The later, post-medieval, kiln remains during the sampling of context 255 are shown on the left. The earlier kiln is shown on the right, during the sampling of context 350. (Photographs courtesy of ASC).

Method

Samples were collected from two contexts, and these were selected to date two kilns from different phases of production at the site (see Figure 1). Samples 01-17 were taken from context 255 which related to one of the later kilns, whilst samples 21-35 came from context 350 which formed part of an earlier structure. All the samples were composed of dark grey vitrified brick but in some cases the upper surface was coated with a white, chalky mortar-like layer. Unfortunately, a number were damaged, either during extraction (12, 13, 15, 17 and 30 which

were not received at the C*f*A) or sample preparation (02 and 10). Context 255 was particularly problematic in this regard, as it appears to have been extremely friable. All samples were collected using the disc method (see appendix, section 1a) and orientated to true north using a gyro-theodolite. The distribution of sample disks over both contexts is shown in Figures 2a and 2b.

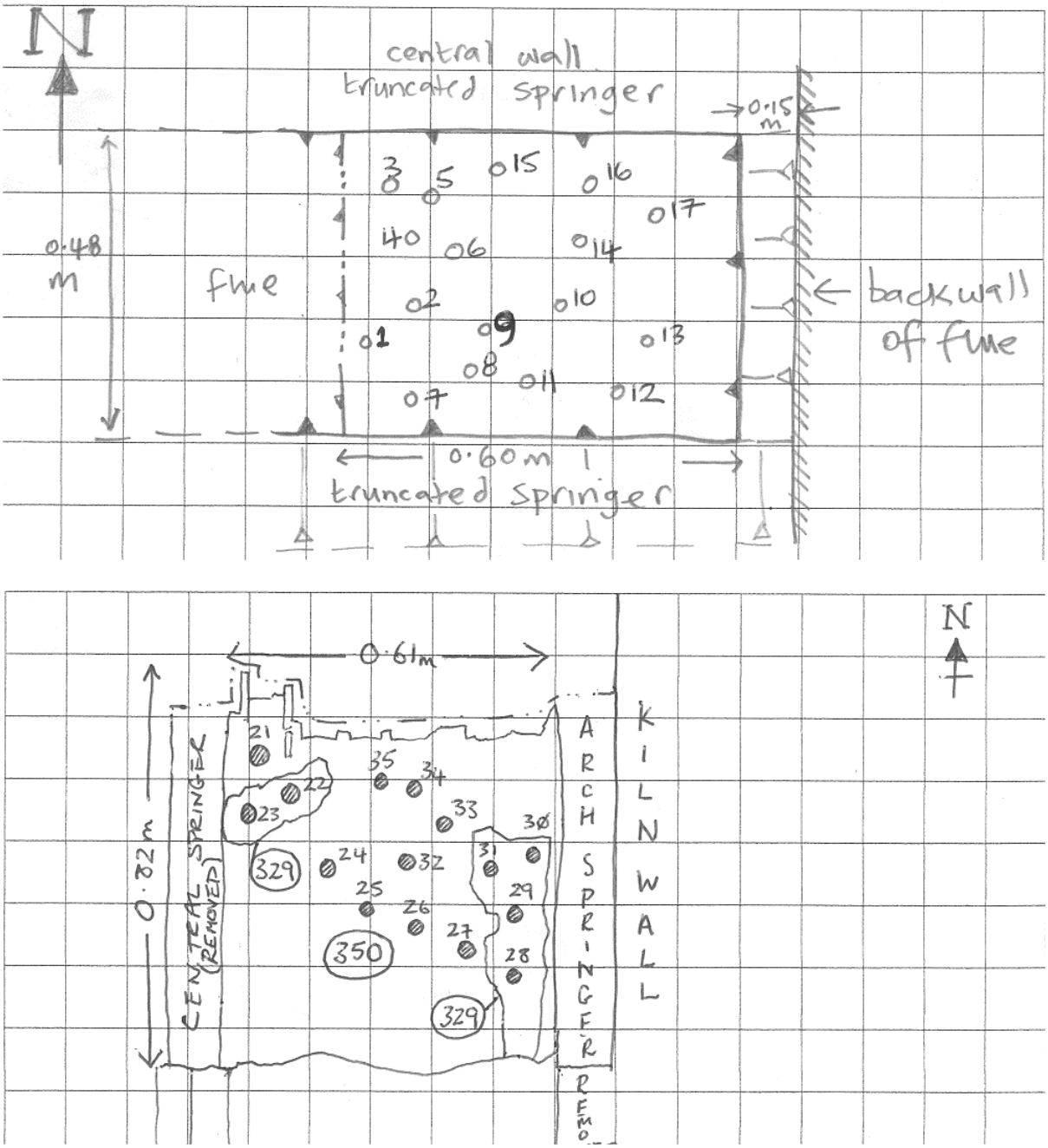

Figure 2: Sketch plans showing sampling locations. The upper diagram shows the locations of samples 1-17 taken from context 255 whilst the lower diagram shows the locations of samples 21-35 taken from context 350. (Plans courtesy of the MoLAS Geomatics Team).

The natural remanent magnetisation (NRM) measured in archaeomagnetic samples is assumed to be caused by thermoremanent magnetisation (TRM) created at the time when the feature of which they were part was last fired. However, a secondary component acquired in later geomagnetic fields can also be present, caused by diagenesis or partial reheating. Additionally, the primary TRM may be overprinted by a viscous component, depending on the grain size distribution within the magnetic material. These secondary components are usually of

lower stability than the primary TRM and can thus be removed by partial demagnetisation of the samples.

To isolate these different components, each sample is partially demagnetised. This involves tumbling the sample in an alternating magnetic field of fixed peak strength and measuring the resulting changes in its magnetisation. This AF demagnetisation removes the contribution of the most weakly magnetised particles within the sample (those with the lowest coercivities). The higher the peak field strength that is applied, the greater the proportion of the sample's magnetisation that is removed. The procedure is repeated with increasing peak field strengths to build up a complete picture of the coercivity spectrum (or demagnetisation curve) for the sample. All measurements are made using the equipment noted in section 2 of the appendix.

Once these measurements have been completed, the consistency of the magnetisation direction recorded in each sample can be assessed using the Maximum Consistency Index (MCI) of Tarling and Symons (1967). This method indicates the range of domain coercivities over which the measured magnetisation direction is most stable. For the sample to be considered to have a stable magnetisation, its MCI should be at least 2 and very stable samples will exhibit an MCI greater than 5.

As an additional test, principal components analysis can be used to determine the various linear segments present within the sample's demagnetisation curve (Kirshvink, 1980). In the ideal case, each linear segment will correspond to one of the magnetisation components described above (primary and, if present, secondary and viscous). Linearity is determined using the Maximum Angular Deviation (MAD) statistic (*ibid*. for definition). The smaller this statistic the better and, as a rule of thumb, sets of measurements with a MAD of <= 2.0° are considered acceptably linear. Once the linear segment corresponding to a sample's primary magnetisation direction has been identified, its principal component is taken as the direction of thermoremanent magnetisation (TRM) recorded by that sample.

A mean TRM direction is then calculated from the directions identified from the partial demagnetisation measurements performed on each sample. Some samples may be excluded from this calculation if their TRM directions are so anomalous as to make them statistical outliers from the overall distribution. A "magnetic refraction" correction can be applied to the sample mean TRM direction to compensate for distortion of the earth's magnetic field due to the geometry of the magnetic fabric of the feature itself. Then the mean is adjusted according to the location of the feature relative to a notional central point in the UK (Meriden), so that it can be compared with UK archaeomagnetic calibration data to produce a date of last firing for the feature. Notes concerning the mean calculation and subsequent calibration can be found in sections 3 and 4 of the appendix.

Results

Context 255 *(samples 01-17)*

The NRM measurements for each sample are contrasted with the final TRM directions determined after partial demagnetisation and principal component analysis in Table 1. These results are depicted graphically in Figure 3. Complete listings of the partial demagnetisation measurements for each sample are provided in Tables 2 to 5. Figures 4 to 6 illustrate the demagnetisation behaviour for selected samples (05, 06 and 09 respectively). Table 6 lists calculations of the maximum consistency index (MCI) for each sample as well as the linearity of the magnetisation direction over successive demagnetisation steps, using principal component analysis with anchored curves (Kirshvink 1980). For both statistics, the mean direction of magnetisation over the most stable range has also been calculated.

Inspection of the NRM results (Figure 3a) indicates that the magnetisation directions of the samples are highly scattered. Even after partial demagnetisation and selection of the most linear components (Figure 3b), the magnetisation directions form only a loose cluster. It may be observed in Table 1 that the strengths of magnetisation of the samples are scattered over three orders of magnitude. Furthermore, there appears to be little correlation between the strength of magnetisation and the stability of the remanent direction. Samples 01, 03 and 09 have very different strengths of magnetisation but all exhibit highly stable directions of magnetisation (demagnetisation results for 09 are depicted graphically in Figure 6). However, sample 05, which was as strongly magnetised as sample 03, and came from the same area, exhibits very poor directional stability (see Figure 4). Hence, the results are somewhat anomalous and the reason is unclear. Likely factors include variability in the heat experienced in different parts of the kiln, heterogeneous magnetic mineral content within the sampled material and variability in the rates that different parts of the context cooled after the final firing. In particular, strongly magnetised areas that cooled rapidly might have perturbed the ambient magnetic field in the vicinity of more slowly cooling areas.

Notwithstanding the above, a mean TRM direction was calculated for context 255. After inspection of the calculations in Table 6, two samples were excluded from the calculation: 07, because its MCI indicated only marginal stability and its remanence direction was highly anomalous and 11 because no acceptably linear component was observed in its partial demagnetisation results. No correction for magnetic refraction was made to the mean direction, as no systematic variation in the magnetisation directions of samples was observed in relation to their position within the feature. The mean TRM direction calculated using the remaining 9 samples is thus:

At site: Dec = 9.7° Inc = 71.9° α_{95} = 4.3° k = 147.5
At Meriden: Dec = 10.1° Inc = 72.4°

From this mean direction, the date for the last firing of the kiln is deduced to be (see Figure 7):

1560 to 1640 AD at the 63% confidence level.
1535 to 1670 AD at the 95% confidence level.

Owing to the nature of the movement of the geomagnetic pole, alternative date ranges are also possible in the Iron Age and Dark Age periods. These have not been calculated as archaeological evidence indicates that the kilns must date from the medieval period at the earliest.

Context 350 (samples 21-35)

The NRM measurements for each sample are contrasted with the final TRM directions determined after partial demagnetisation and principal component analysis in Table 7. These results are depicted graphically in Figure 8. Complete listings of the partial demagnetisation measurements for each sample are provided in Tables 8 to 12. Figures 9 to 11 illustrate the demagnetisation behaviour for selected samples (21, 24 and 28 respectively). Table 13 lists calculations of the maximum consistency index (MCI) for each sample as well as the linearity of the magnetisation direction over successive demagnetisation steps, using principal components analysis with anchored curves (Kirshvink 1980). For both statistics, the mean direction of magnetisation over the most stable range has also been calculated.

Inspection of Figure 8 indicates that the directions of remanent magnetisation in the samples from context 350 were far more consistent, even the NRM results are tightly clustered. On demagnetisation all the samples exhibited highly consistent and linear behaviour, that illustrated in Figure 11 for sample 28 being typical. A harder component was noted in the demagnetisation results of samples 24, 27 and 32 (although it is present to a lesser extent in

some other samples) and this can be observed in Figure 10 depicting the results from sample 24.

A mean TRM direction was calculated using the components of maximum linearity from all samples taken from context 350. Technically, applying the analysis of Beck (1983), sample 21 was a statistical outlier. However, there were no good grounds for excluding it as its magnetisation direction was stable and linear (see Figure 9). Hence it was not excluded from the calculation. No correction for magnetic refraction was made to the mean direction, as no systematic variation in the magnetisation directions of samples was observed in relation to their position within the feature. The mean TRM direction calculated from all 14 samples is thus:

At site: Dec = 2.7° Inc = 63.6° α_{95} = 1.6° k = 639.8
At Meriden: Dec = 2.6° Inc = 64.2°

This direction lies some 4-5º to the west of the early post-medieval segment of the calibration curve, overlying the Roman segment. However, stratigraphic evidence excludes such an early date and indicates that the feature must date from the medieval or early post-medieval period. It may be noted in plans of the kiln from which these samples were taken that its long axis runs about 10º west of true north. It is possible that the declination of the Earth's magnetic field in the vicinity of the strongly magnetised structure was perturbed slightly to the west to align more closely with this long axis. This is in much the same way that a needle always magnetises along its length rather than transversely. With this assumption, the mean TRM direction was projected East onto the early post-medieval segment of the curve. It was further assumed that no perturbation to the inclination of the TRM direction occurred. With this *caveat*, the date for the last firing of the kiln is deduced to be:

No date possible at the 63% confidence level.
1440 to 1480 AD at the 95% confidence level.

Given the assumption that had to be made to produce a date for this feature, it was not deemed appropriate to calculate a date range at the narrower, 63% confidence level.

Conclusions

Archaeomagnetic dates have been determined for both the features sampled at Rose Cottage but the results need some qualification. The stratigraphically earlier context, 350, was dated to 1440-1480 AD at the 95% confidence level. This was based upon a mean TRM determination of high precision. However, the direction of this mean was about 4-5° to the west of the medieval/port-medieval segment of the calibration curve. It was assumed that this was due to distortion of the Earth's magnetic field due to the shape of the magnetised kiln structure. To derive the date it has been assumed that this distortion only affected the declination of the TRM recorded in the samples and the mean direction has been projected due eastwards (see Figure 12) onto the relevant portion of the calibration curve. Thus it should be borne in mind that the date might not be accurate if this assumption is incorrect.

Context 255 exhibited a surprisingly high degree of scattering of individual TRM directions for what appeared to be a well fired surface. It has been assumed that the magnetic material within the brick fabric has an inhomogeneous distribution and that the cooling of this area after firing was uneven. This has resulted in a mean TRM direction of poor precision which, in turn, has produced a wide date range for the feature.

Nevertheless, it is clear from the archaeomagnetic dates that the last firing of context 255 postdates that of context 350 by a century or more. Furthermore, both dates seem to be later than the main phase of decorated tile production at Penn in the 1300s.

P. Linford
Archaeometry Branch,
Centre for Archaeology, English Heritage.

Date of report: 27/11/2003

Archaeomagnetic Date Summary

Archaeomagnetic ID:	**1PTG**
Feature:	**Tile Kiln, Tyler's Green, site code PTG03**
Context(s):	**255**
Location:	**Longitude 0.7°W, Latitude 51.6°N**
Number of Samples (taken/used in mean):	**11/9**
AF Demagnetisation Applied:	**up to 20-50mT (see tables)**
Distortion Correction Applied:	**None**
Declination (at Meriden):	**9.7° (10.1°)**
Inclination (at Meriden):	**71.9° (72.4°)**
Alpha-95:	**4.3°**
k:	**147.5**
Date range (63% confidence):	**1560 AD to 1640 AD**
Date range (95% confidence):	**1535 AD to 1670 AD**
Independent date estimate:	**post-medieval, possibly C17th AD**

Archaeomagnetic ID:	**2PTG**
Feature:	**Tile Kiln, Tyler's Green, site code PTG03**
Context(s):	**350**
Location:	**Longitude 0.7°W, Latitude 51.6°N**
Number of Samples (taken/used in mean):	**14/14**
AF Demagnetisation Applied:	**75mT (see tables)**
Distortion Correction Applied:	**None**
Declination (at Meriden):	**2.7° (2.6°)**
Inclination (at Meriden):	**63.6° (64.2°)**
Alpha-95:	**1.6°**
k:	**639.8**
Date range (63% confidence):	**Undatable (see text)**
Date range (95% confidence):	**1440 AD to 1480 AD**
Independent date estimate:	**?medieval**

	NRM Measurements				After Partial Demagnetisation				
Sample	Material	Dec°	Inc°	J(mAm^{-1})	AF(mT)	Dec°	Inc°	MAD°	R
01	brick	30.5	79.2	136.6	50.0	18.2	75.6	1.5	
03	brick	12.1	71.9	6558.6	50.0	11.5	71.7	0.8	
04	brick	-7.6	39.4	692.1	50.0	-4.1	66.8	1.6	
05	brick	-73.9	72.0	3348.3	50.0	-6.8	79.8	1.1	
06	brick	24.2	70.6	4747.5	50.0	8.7	75.4	1.2	
07	brick	86.1	47.5	13.2	30.0	110.4	32.1	0.5	R
08	brick	-7.3	54.1	6.7	20.0	13.0	62.0	0.7	
09	brick	37.7	68.8	75.7	50.0	35.8	68.9	1.5	
11	brick	-31.3	78.8	15.9	30.0	-	-	-	R
14	brick	19.6	73.8	2351.0	50.0	6.3	71.4	1.6	
16	brick	4.4	70.3	3651.1	50.0	-2.0	71.9	1.7	

Table 1: NRM measurements of samples and measurements after partial AF demagnetisation for feature 1PTG. J = magnitude of magnetisation vector; AF = peak alternating field strength of demagnetising field; MAD = Maximum Angular Deviation (see text); R = sample rejected from mean calculation.

	01			03			04		
AF(mT)	Dec°	Inc°	J(mAm^{-1})	Dec°	Inc°	J(mAm^{-1})	Dec°	Inc°	J(mAm^{-1})
0.0	30.5	79.2	136.6	12.1	71.9	6558.6	-7.6	39.4	692.1
1.0	26.1	78.9	134.1	10.4	71.9	5963.9	-6.7	52.9	691.7
2.5	26.7	79.3	128.1	11.1	71.8	5879.7	-5.9	56.6	660.6
5.0	33.6	79.3	114.7	10.6	72.0	5621.9	-5.1	61.1	567.9
7.5	36.5	80.5	99.7	9.9	72.3	5239.1	-3.8	63.5	481.7
10.0	42.8	80.9	85.6	10.1	72.3	4884.1	1.1	64.4	420.7
15.0	58.4	82.9	62.5	10.0	72.3	4215.2	-9.8	62.0	322.5
20.0	91.7	84.6	44.6	9.8	72.5	3787.1	-3.8	66.5	266.7
30.0	137.7	74.6	24.6	8.8	72.6	3157.0	-2.4	67.3	199.3
50.0	165.4	38.9	8.9	9.2	73.1	2222.5	3.7	66.0	111.4

Table 2: Incremental partial demagnetisation measurements for samples 01, 03 and 04 from feature 1PTG.

	05			06			07		
AF(mT)	Dec°	Inc°	J(mAm^{-1})	Dec°	Inc°	J(mAm^{-1})	Dec°	Inc°	J(mAm^{-1})
0.0	-73.9	72.0	3348.3	24.2	70.6	4747.5	86.1	47.5	13.2
1.0	-43.0	78.4	3193.3	15.3	73.0	4201.1	85.8	45.6	12.4
2.5	-32.5	77.8	3022.3	12.9	74.1	3872.6	91.2	48.8	11.3
5.0	-23.8	78.0	2571.0	9.2	75.2	3302.1	91.0	48.7	9.4
7.5	-15.4	78.3	2062.3	7.5	75.9	2884.1	98.8	47.2	8.1
10.0	-30.6	73.2	1688.3	7.0	76.2	2576.1	93.2	51.5	6.2
15.0	-28.4	74.0	1251.2	5.8	76.7	2086.0	74.5	61.7	4.0
20.0	-7.2	79.5	1052.1	5.4	76.7	1801.8	71.9	62.2	2.5
30.0	-4.9	79.9	792.8	5.5	77.0	1387.7	22.9	77.4	1.9
50.0	-4.7	77.7	449.0	4.9	77.5	822.2	-	-	-

Table 3: Incremental partial demagnetisation measurements for samples 05, 06 and 07 from feature 1PTG.

	08			09			11		
AF(mT)	Dec°	Inc°	J(mAm^{-1})	Dec°	Inc°	J(mAm^{-1})	Dec°	Inc°	J(mAm^{-1})
0.0	-7.3	54.1	6.7	37.7	68.8	75.7	-31.3	78.8	15.9
1.0	-11.6	56.2	6.3	35.7	70.0	69.6	-30.2	77.2	14.7
2.5	-17.3	53.5	4.9	35.9	69.5	66.0	-44.6	75.0	12.7
5.0	-21.1	51.8	4.2	35.1	69.5	60.0	-47.3	73.0	9.6
7.5	-18.4	50.9	3.6	38.8	68.8	52.6	-42.6	71.9	7.2
10.0	-25.1	51.0	2.9	37.4	69.8	46.7	-53.0	70.6	5.3
15.0	-34.3	40.6	2.5	37.4	70.1	37.2	-57.7	58.3	4.2
20.0	-28.4	33.9	2.9	35.9	71.2	29.8	-53.7	52.8	2.5
30.0	-	-	-	37.9	71.2	21.0	-67.7	60.1	2.2
50.0	-	-	-	51.6	72.4	12.2	-	-	-

Table 4: Incremental partial demagnetisation measurements for samples 08, 09 and 11 from feature 1PTG.

	14			16		
AF(mT)	Dec°	Inc°	J(mAm^{-1})	Dec°	Inc°	J(mAm^{-1})
0.0	19.6	73.8	2351.0	4.4	70.3	3651.1
1.0	11.0	73.1	2340.8	-1.2	71.8	3365.4
2.5	8.8	72.5	2261.7	-3.2	72.3	3192.6
5.0	6.4	71.6	2092.1	-4.3	72.8	2888.0
7.5	5.5	71.3	1932.5	-4.6	72.9	2584.5
10.0	4.4	71.2	1799.2	-5.9	73.2	2345.2
15.0	2.7	71.0	1589.6	-6.5	73.7	1985.6
20.0	1.7	70.3	1442.2	-6.0	73.7	1709.1
30.0	1.3	71.3	1210.6	-8.4	74.2	1313.5
50.0	-0.4	70.7	884.1	-7.8	73.9	805.5

Table 5: Incremental partial demagnetisation measurements for samples 14 and 16 from feature 1PTG.

	Consistency						Linearity					
Sample	Min	Max	N	MCI	Dec°	Inc°	Min	Max	N	MAD°	Dec°	Inc°
01	0.0	5.0	4	10.3	29.2	79.2	0.0	50.0	10	1.5	18.2	75.6
03	7.5	15.0	3	284.9	10.0	72.3	0.0	zero	11	0.8	11.5	71.7
04	20.0	50.0	3	10.1	-0.8	66.6	20.0	zero	4	1.6	-4.1	66.8
05	20.0	50.0	3	14.4	-5.6	79.0	20.0	zero	4	1.1	-6.8	79.8
06	15.0	30.0	3	68.2	5.6	76.8	5.0	zero	8	1.2	8.7	75.4
07	2.5	10.0	4	2.9	93.6	49.1	7.5	15.0	3	0.5	110.4	32.1
08	2.5	7.5	3	4.0	-19.0	52.1	1.0	5.0	3	0.7	13.0	62.0
09	1.0	5.0	3	19.6	35.6	69.7	0.0	zero	11	1.5	35.8	68.9
14	15.0	50.0	4	31.1	1.3	70.8	5.0	zero	8	1.6	6.3	71.4
16	15.0	50.0	4	48.1	-7.2	73.9	1.0	zero	10	1.7	-2.0	71.9

Table 6: Assessment of the range of demagnetisation values over which each sample attained its maximum directional consistency and linearity for feature 1PTG. Consistency is calculated using the method of Tarling and Symons (1967) and linearity using the method of Kirshvink (1980). Min and Max indicate the range of demagnetisation values in mT over which each statistic was calculated and N is the number of consecutive measurements this represents. MCI is the maximum value of Tarling and Symons' consistency index found for the sample (over 2 for a stable magnetisation). MAD is Kirshvink's maximum angular deviation (less than 2^o indicates linearity). In each case, declination and inclination values are for the mean direction calculated from all demagnetisation measurements in the range indicated.

	NRM Measurements				After Partial Demagnetisation				
Sample	Material	Dec°	Inc°	J(mAm^{-1})	AF(mT)	Dec°	Inc°	MAD°	R
21	brick	-1.7	57.7	4107.7	75.0	-1.6	58.4	1.0	
22	brick	5.8	63.1	613.6	75.0	5.1	62.4	0.7	
23	brick	0.3	61.8	254.9	75.0	1.1	62.2	0.7	
24	brick	6.7	61.0	5128.7	75.0	6.9	61.2	0.7	
25	brick	1.5	59.8	629.9	75.0	2.1	60.7	1.7	
26	brick	0.7	67.1	323.1	75.0	-0.2	67.4	0.8	
27	brick	-1.4	66.5	4210.8	75.0	-0.9	66.6	0.5	
28	brick	3.4	61.6	434.2	75.0	4.0	62.0	0.8	
29	brick	6.6	60.7	864.1	75.0	7.2	61.0	0.8	
31	brick	2.2	62.9	1070.9	75.0	1.9	63.3	0.6	
32	brick	5.3	66.1	4719.5	75.0	6.4	66.5	0.7	
33	brick	5.7	66.9	539.5	75.0	6.0	66.6	1.3	
34	brick	0.1	66.0	1029.6	75.0	0.9	66.7	1.1	
35	brick	-1.8	65.0	710.4	75.0	-1.7	65.0	0.7	

Table 7: NRM measurements of samples and measurements after partial AF demagnetisation for feature 2PTG. J = magnitude of magnetisation vector; AF = peak alternating field strength of demagnetising field; MAD = Maximum Angular Deviation (see text); R = sample rejected from mean calculation.

	21			22			23		
AF(mT)	Dec°	Inc°	J(mAm^{-1})	Dec°	Inc°	J(mAm^{-1})	Dec°	Inc°	J(mAm^{-1})
0.0	-1.7	57.7	4107.7	5.8	63.1	613.6	0.3	61.8	254.9
1.0	-1.9	58.1	4127.8	5.6	62.9	613.3	0.4	61.8	253.1
2.5	-1.8	58.1	4167.2	6.4	63.0	612.3	0.8	61.9	249.7
5.0	-2.0	58.2	4176.4	6.3	63.1	599.6	1.2	61.9	237.3
10.0	-2.5	58.0	3999.4	7.7	64.7	534.0	1.6	61.7	202.4
15.0	-2.8	57.9	3543.5	4.7	62.5	442.7	1.1	61.8	164.8
20.0	-3.4	57.5	3211.6	4.9	62.3	372.4	0.9	61.2	129.2
30.0	-3.9	57.4	2606.4	3.3	62.0	270.1	-0.3	60.4	84.8
50.0	-4.2	56.4	1488.9	2.0	62.2	161.9	-2.4	58.0	43.8
75.0	-4.5	54.5	657.9	1.9	62.8	94.1	-4.1	59.3	23.6

Table 8: Incremental partial demagnetisation measurements for samples 21, 22 and 23 from feature 2PTG.

	24			25			26		
AF(mT)	Dec°	Inc°	J(mAm^{-1})	Dec°	Inc°	J(mAm^{-1})	Dec°	Inc°	J(mAm^{-1})
0.0	6.7	61.0	5128.7	1.5	59.8	629.9	0.7	67.1	323.1
1.0	7.1	61.0	5127.7	2.2	60.7	630.3	-1.0	67.5	326.4
2.5	6.9	61.0	5128.3	3.0	61.0	629.7	-0.6	67.2	323.7
5.0	6.8	61.0	5124.8	2.8	61.4	626.5	-1.1	67.4	321.0
10.0	7.3	60.9	5106.0	3.6	61.8	567.7	-1.0	67.6	305.8
15.0	6.6	60.8	4986.3	4.0	61.5	479.8	-1.2	67.5	278.4
20.0	7.0	60.6	4766.2	4.7	61.8	409.6	-1.3	67.5	253.5
30.0	7.1	60.2	4036.5	5.4	62.1	314.3	-1.4	67.5	206.4
50.0	6.9	59.7	2459.2	5.6	61.9	197.3	-2.2	66.5	138.3
75.0	6.7	59.5	1133.9	4.4	62.1	117.1	-2.9	67.4	86.8

Table 9: Incremental partial demagnetisation measurements for samples 24, 25 and 26 from feature 2PTG.

	27			28			29		
AF(mT)	Dec°	Inc°	J(mAm^{-1})	Dec°	Inc°	J(mAm^{-1})	Dec°	Inc°	J(mAm^{-1})
0.0	-1.4	66.5	4210.8	3.4	61.6	434.2	6.6	60.7	864.1
1.0	-0.3	66.4	4239.1	3.3	61.8	432.7	7.0	60.8	865.8
2.5	-0.6	66.7	4249.6	3.6	62.1	429.7	7.2	60.7	857.9
5.0	-	-	-	4.3	62.4	414.9	6.9	61.2	841.9
10.0	-	-	-	4.0	62.4	364.0	7.6	60.6	753.0
15.0	-1.5	66.5	4059.3	4.2	62.3	305.5	6.6	60.3	651.7
20.0	-0.9	66.6	3859.2	3.1	62.1	255.9	7.1	59.9	558.1
30.0	-1.3	66.6	3252.5	3.2	61.9	186.1	6.3	59.9	433.5
50.0	-1.4	66.4	1952.8	3.2	62.2	117.8	6.4	60.2	297.8
75.0	-1.3	65.7	865.7	-1.2	61.9	71.8	5.9	59.8	185.2

Table 10: Incremental partial demagnetisation measurements for samples 27, 28 and 29 from feature 2PTG.

	31			32			33		
AF(mT)	Dec°	Inc°	J(mAm^{-1})	Dec°	Inc°	J(mAm^{-1})	Dec°	Inc°	J(mAm^{-1})
0.0	2.2	62.9	1070.9	5.3	66.1	4719.5	5.7	66.9	539.5
1.0	1.8	63.2	1065.7	6.4	66.2	4737.5	5.5	66.4	545.9
2.5	1.4	63.3	1074.3	6.4	66.2	4739.4	5.7	66.5	545.5
5.0	1.7	63.2	1054.9	6.7	66.2	4732.8	5.0	66.2	544.3
10.0	2.2	63.3	964.3	6.8	66.4	4663.9	4.9	66.0	525.5
15.0	2.6	63.2	864.2	6.8	66.2	4488.4	3.9	65.8	482.9
20.0	1.9	62.9	761.7	7.2	66.4	4277.9	3.4	65.6	436.0
30.0	1.3	62.9	604.9	7.3	66.4	3609.2	3.3	65.2	337.9
50.0	1.5	62.6	419.8	6.7	65.9	2130.3	2.4	65.0	209.1
75.0	2.0	62.6	271.9	7.0	63.5	764.7	0.5	65.0	135.4

Table 11: Incremental partial demagnetisation measurements for samples 31, 32 and 33 from feature 2PTG.

	34			35		
AF(mT)	Dec°	Inc°	J(mAm^{-1})	Dec°	Inc°	J(mAm^{-1})
0.0	0.1	66.0	1029.6	-1.8	65.0	710.4
1.0	1.4	66.7	1027.9	-1.9	65.0	715.6
2.5	1.4	66.9	1020.1	-1.3	64.7	714.5
5.0	1.9	66.8	1004.7	-1.1	64.9	710.8
10.0	2.4	66.6	954.5	-1.5	64.6	682.4
15.0	2.7	66.6	884.8	-1.1	64.2	631.2
30.0	4.2	66.6	630.6	-0.6	64.2	430.0
50.0	4.5	66.4	352.2	-0.3	64.1	245.8
75.0	4.5	65.8	171.4	-0.4	63.4	132.6

Table 12: Incremental partial demagnetisation measurements for samples 34 and 35 from feature 2PTG.

	Consistency						Linearity					
Sample	Min	Max	N	MCI	Dec°	Inc°	Min	Max	N	MAD°	Dec°	Inc°
21	1.0	5.0	3	80.9	-1.9	58.1	0.0	zero	11	1.0	-1.6	58.4
22	30.0	75.0	3	38.4	2.4	62.3	15.0	zero	6	0.7	5.1	62.4
23	5.0	15.0	3	62.4	1.3	61.8	0.0	zero	11	0.7	1.1	62.2
24	0.0	5.0	4	85.4	6.9	61.0	0.0	zero	11	0.7	6.9	61.2
25	20.0	75.0	4	76.7	5.0	62.0	0.0	zero	11	1.7	2.1	60.7
26	15.0	30.0	3	320.2	-1.3	67.5	0.0	zero	11	0.8	-0.2	67.4
27	15.0	50.0	4	131.9	-1.3	66.5	0.0	zero	9	0.5	-0.9	66.6
28	20.0	50.0	3	111.7	3.2	62.1	0.0	zero	11	0.8	4.0	62.0
29	30.0	75.0	3	86.0	6.2	60.0	0.0	zero	11	0.8	7.2	61.0
31	20.0	75.0	4	102.0	1.7	62.8	0.0	zero	11	0.6	1.9	63.3
32	1.0	50.0	8	103.6	6.8	66.2	0.0	zero	11	0.7	6.4	66.5
33	20.0	50.0	3	45.2	3.0	65.3	0.0	zero	11	1.3	6.0	66.6
34	5.0	15.0	3	50.7	2.3	66.7	0.0	zero	10	1.1	0.9	66.7
35	15.0	50.0	3	101.0	-0.7	64.2	0.0	zero	10	0.7	-1.7	65.0

Table 13: Assessment of the range of demagnetisation values over which each sample attained its maximum directional consistency and linearity for feature 2PTG. Consistency is calculated using the method of Tarling and Symons (1967) and linearity using the method of Kirshvink (1980). Min and Max indicate the range of demagnetisation values in mT over which each statistic was calculated and N is the number of consecutive measurements this represents. MCI is the maximum value of Tarling and Symons' consistency index found for the sample (over 2 for a stable magnetisation). MAD is Kirshvink's maximum angular deviation (less than 2^o indicates linearity). In each case, declination and inclination values are for the mean direction calculated from all demagnetisation measurements in the range indicated.

Appendix: Standard Procedures for Sampling and Measurement

1) Sampling

One of three sampling techniques is employed depending on the consistency of the material (Clark, Tarling and Noel 1988):

a) **Consolidated materials:** Rock and fired clay samples are collected by the disc method. Several small levelled plastic discs are glued to the feature, marked with an orientation line related to True North, then removed with a small piece of the material attached.

b) **Unconsolidated materials:** Sediments are collected by the tube method. Small pillars of the material are carved out from a prepared platform, then encapsulated in levelled plastic tubes using plaster of Paris. The orientation line is then marked on top of the plaster.

c) **Plastic materials:** Waterlogged clays and muds are sampled in a similar manner to method 1b) above; however, the levelled plastic tubes are pressed directly into the material to be sampled.

2) Physical Analysis

a) Magnetic remanences are measured using a slow speed spinner fluxgate magnetometer (Molyneux et al. 1972; see also Tarling 1983, p84; Thompson and Oldfield 1986, p52).

b) Partial demagnetisation is achieved using the alternating magnetic field method (As 1967; Creer 1959; see also Tarling 1983, p91; Thompson and Oldfield 1986, p59), to remove viscous magnetic components if necessary. Demagnetising fields are measured in milli-Tesla (mT), figures quoted being for the peak value of the field.

3) Remanent Field Direction

a) The remanent field direction of a sample is expressed as two angles, declination (Dec) and inclination (Inc), both quoted in degrees. Declination represents the bearing of the field relative to true north, angles to the east being positive; inclination represents the angle of dip of this field.

b) Aitken and Hawley (1971) have shown that the angle of inclination in measured samples is likely to be distorted owing to magnetic refraction. The phenomenon is not well understood but is known to depend on the position the samples occupied within the structure. The corrections recommended by Aitken and Hawley are applied, where appropriate, to measured inclinations, in keeping with the practice of Clark, Tarling and Noel (1988).

c) Individual remanent field directions are combined to produce the mean remanent field direction using the statistical method developed by R. A. Fisher (1953). The quantity α_{95}, "alpha-95", is quoted with mean field directions and is a measure of the precision of the determination (see Aitken 1990, p247). It is analogous to the standard error statistic for scalar quantities; hence the smaller its value, the better the precision of the date.

d) For the purposes of comparison with standardised UK calibration data, remanent field directions are adjusted to the values they would have had if the feature had been located at Meriden, a standard reference point. The adjustment is done using the method suggested by Noel (Tarling 1983, p116).

4) Calibration

a) Material less than 3000 years old is dated using the archaeomagnetic calibration curve compiled by Clark, Tarling and Noel (1988).

b) Older material is dated using the lake sediment data compiled by Turner and Thompson (1982).

c) Dates are normally given at the 63% and 95% confidence levels. However, the quality of the measurement and the estimated reliability of the calibration curve for the period in question are not taken into account, so this figure is only approximate. Owing to crossovers and contiguities in the curve, alternative dates are sometimes given. It may be possible to select the correct alternative using independent dating evidence.

d) As the thermoremanent effect is reset at each heating, all dates for fired material refer to the final heating.

References

Aitken, M. J. 1990. *Science-based Dating in Archaeology*. London: Longman.

Aitken, M. J. and H. N. Hawley 1971. Archaeomagnetism: evidence for magnetic refraction in kiln structures. *Archaeometry* **13**, 83-85.

As, J. A. 1967. The a.c. demagnetisation technique, in *Methods in Palaeomagnetism*, D. W. Collinson, K. M. Creer and S. K. Runcorn (eds). Amsterdam: Elsevier.

Beck, M. E. 1983. Comment on: 'Determination of the angle of a Fisher distribution which will be exceeded with a given probability' by P. L. McFadden. *Geophys. J. R. Astr., Soc*. **75**, 847-849.

Clark, A. J., Tarling, D. H. and Noel, M. 1988. Developments in Archaeomagnetic Dating in Britain. *J. Arch. Sci.* **15**, 645-667.

Creer, K. M. 1959. A.C. demagnetisation of unstable Triassic Keuper Marls from S. W. England. *Geophys. J. R. Astr. Soc.* **2**, 261-275.

Fell, D., 2001. An Archaeological Evaluation at Rose Cottage, Tyler's Green, Buckinghamshire. *Unpublished Archaeological Services and Consultancy Ltd. report* **ASC: TGR01/2**.

Fisher, R. A. 1953. Dispersion on a sphere. *Proc. R. Soc. London A* **217**, 295-305.

Kirshvink, J. L. 1980. The least-squares line and plane and the analysis of palaeomagnetic data. *Geophys. J. R. Astr., Soc*. **62**, 699-718.

Molyneux, L., Thompson, R., Oldfield, F. and McCallan, M. E. 1972. Rapid measurement of the remanent magnetisation of long cores of sediment. *Nature* **237**, 42-43.

Tarling, D. H. 1983. *Palaeomagnetism*. London: Chapman and Hall.

Tarling, D. H. and Symons, D. T. A. 1967. A stability index of remanence in palaeomagnetism. *Geophys. J. R. Astr., Soc*. **12**, 443-448.

Thompson, R. and Oldfield, F. 1986. *Environmental Magnetism*. London: Allen and Unwin.

Turner, G. M. and Thompson, R. 1982. Detransformation of the British geomagnetic secular variation record for Holocene times. *Geophys. J. R. Astr. Soc.* **70**, 789-792.

a)

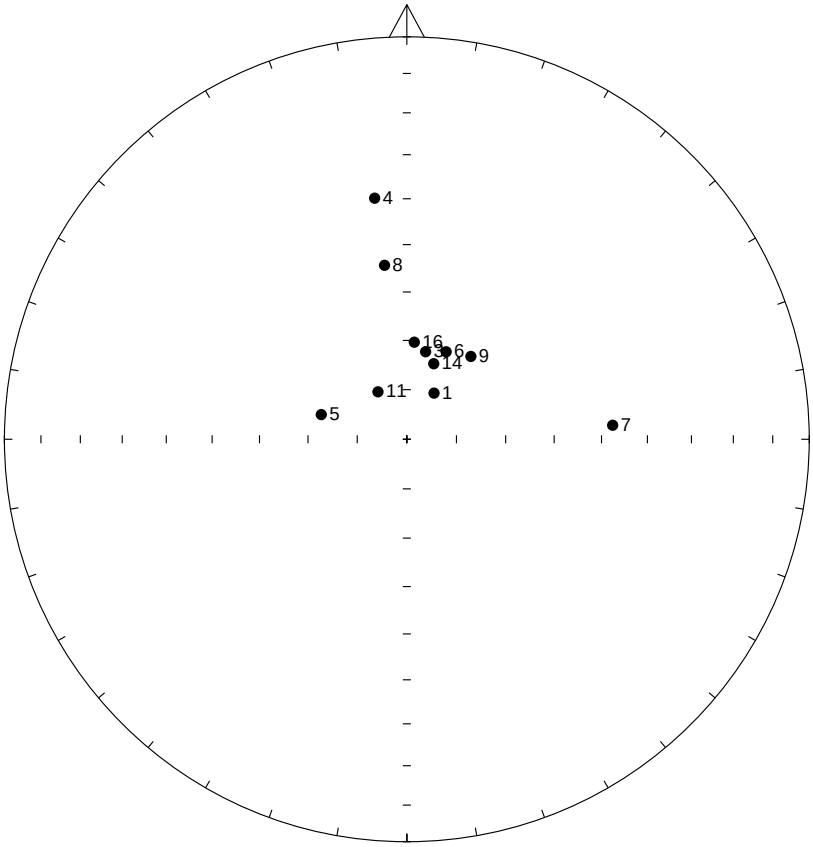

b)

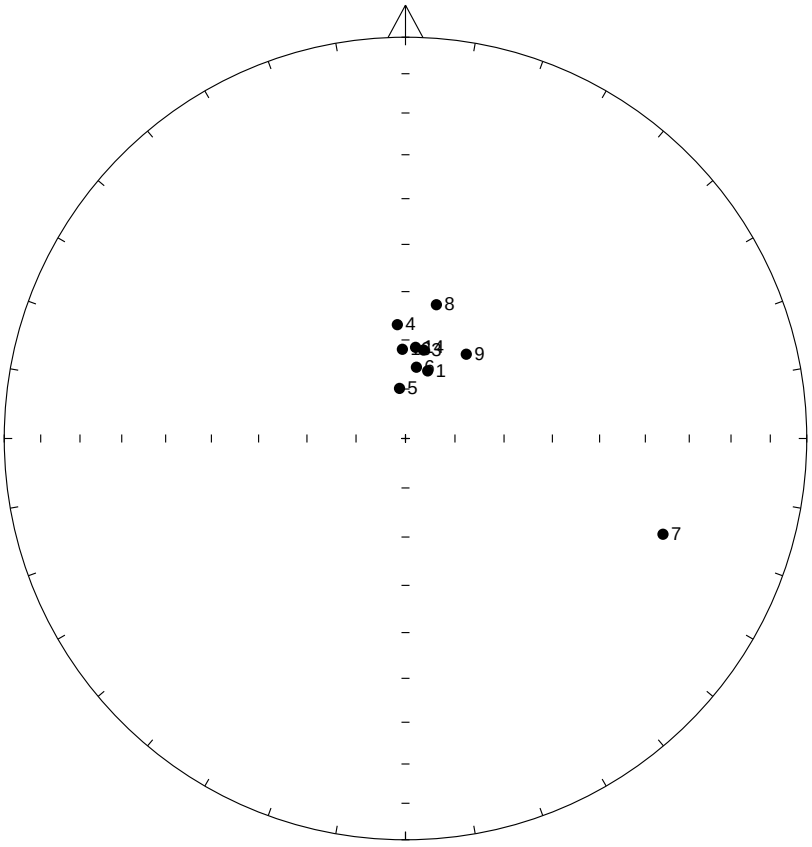

Figure 3: a) Distribution of NRM directions of samples from context 255 represented as an equal area stereogram. In this projection declination increases clockwise with zero being at 12 o'clock while inclination increases from zero at the equator to 90 degrees in the centre of the projection. Open circles represent negative inclinations. b) Distribution of thermoremanent directions of magnetisation of the same samples after partial AF demagnetisation.

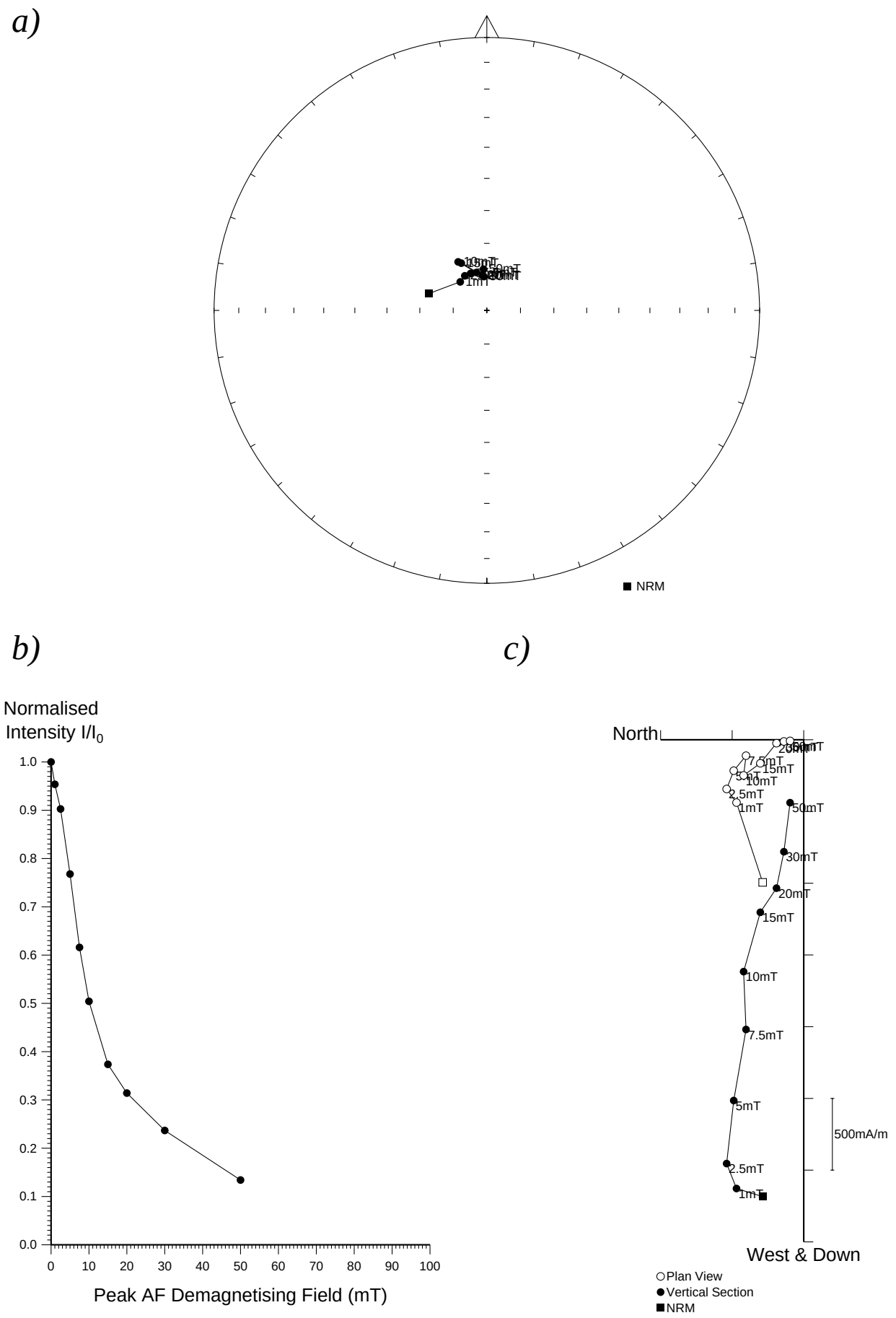

Figure 4: Stepwise AF demagnetisation of sample 05. Diagram a) depicts the variation of the remanent direction as an equal area stereogram (declination increases clockwise, while inclination increases from zero at the equator to 90 degrees at the centre of the projection); b) shows the normalised change in remanence intensity as a function of the demagnetising field; c) shows the changes in both direction and intensity as a vector endpoint projection.

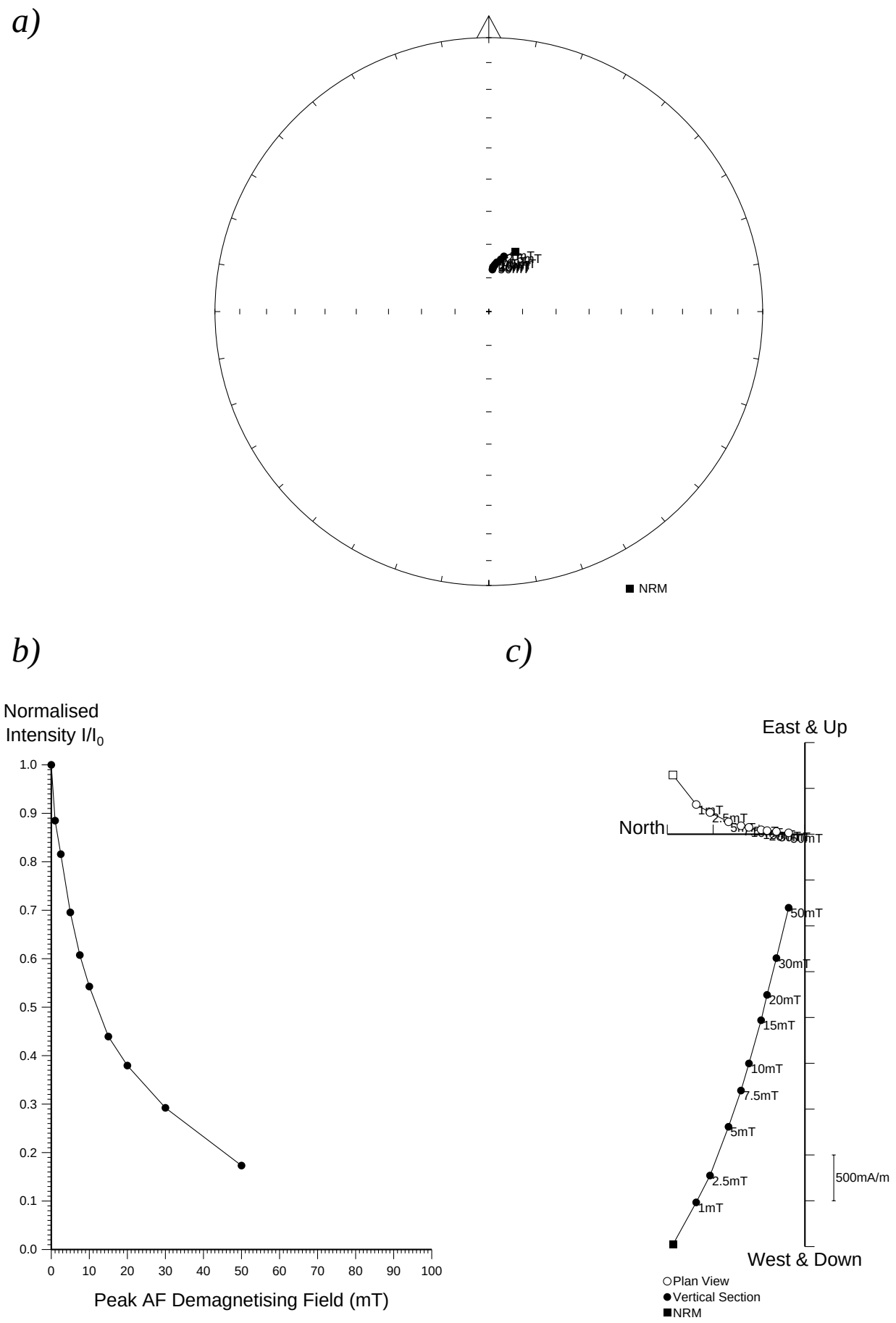

Figure 5: Stepwise AF demagnetisation of sample 06. Diagram a) depicts the variation of the remanent direction as an equal area stereogram (declination increases clockwise, while inclination increases from zero at the equator to 90 degrees at the centre of the projection); b) shows the normalised change in remanence intensity as a function of the demagnetising field; c) shows the changes in both direction and intensity as a vector endpoint projection.

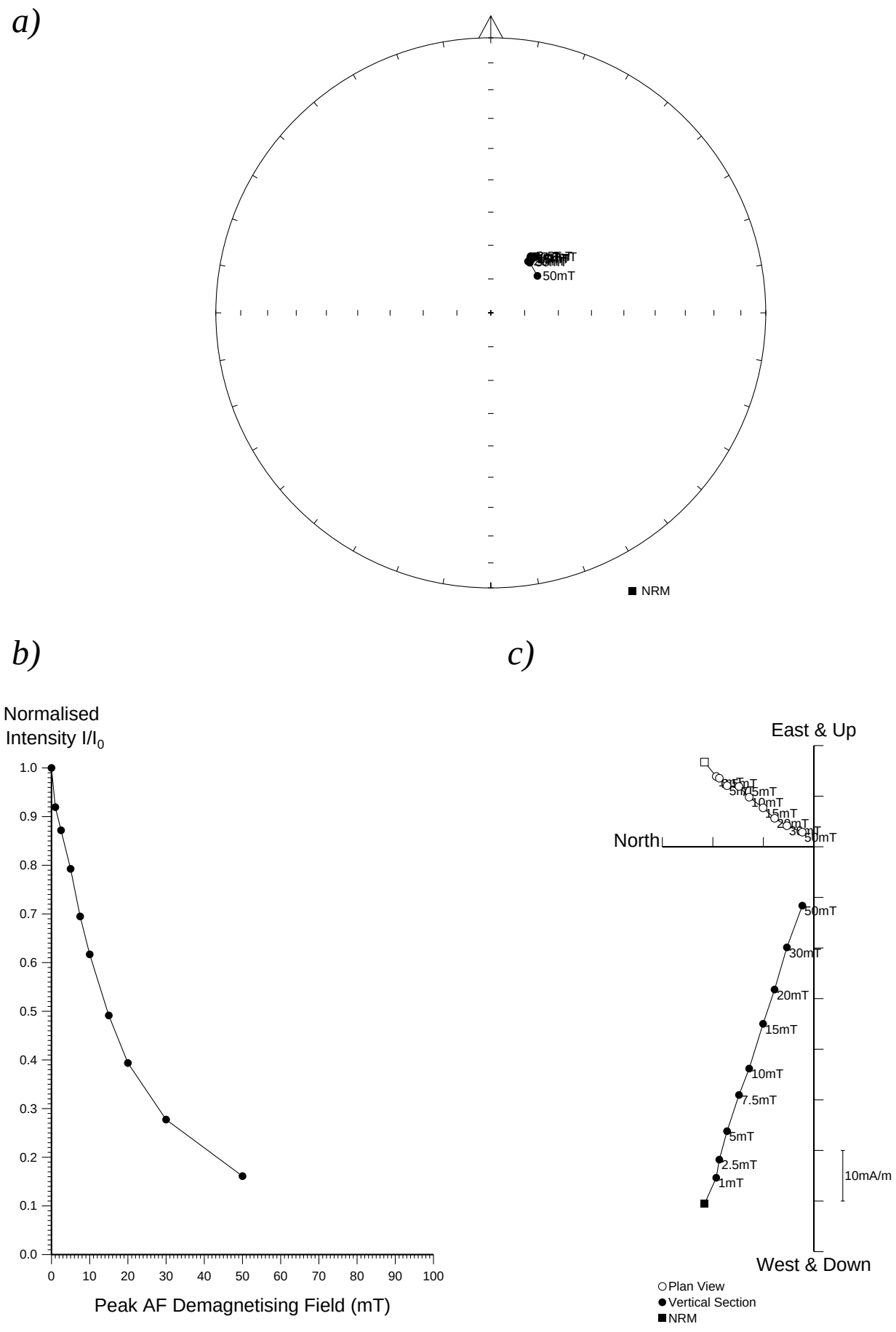

Figure 6: Stepwise AF demagnetisation of sample 09. Diagram a) depicts the variation of the remanent direction as an equal area stereogram (declination increases clockwise, while inclination increases from zero at the equator to 90 degrees at the centre of the projection); b) shows the normalised change in remanence intensity as a function of the demagnetising field; c) shows the changes in both direction and intensity as a vector endpoint projection.

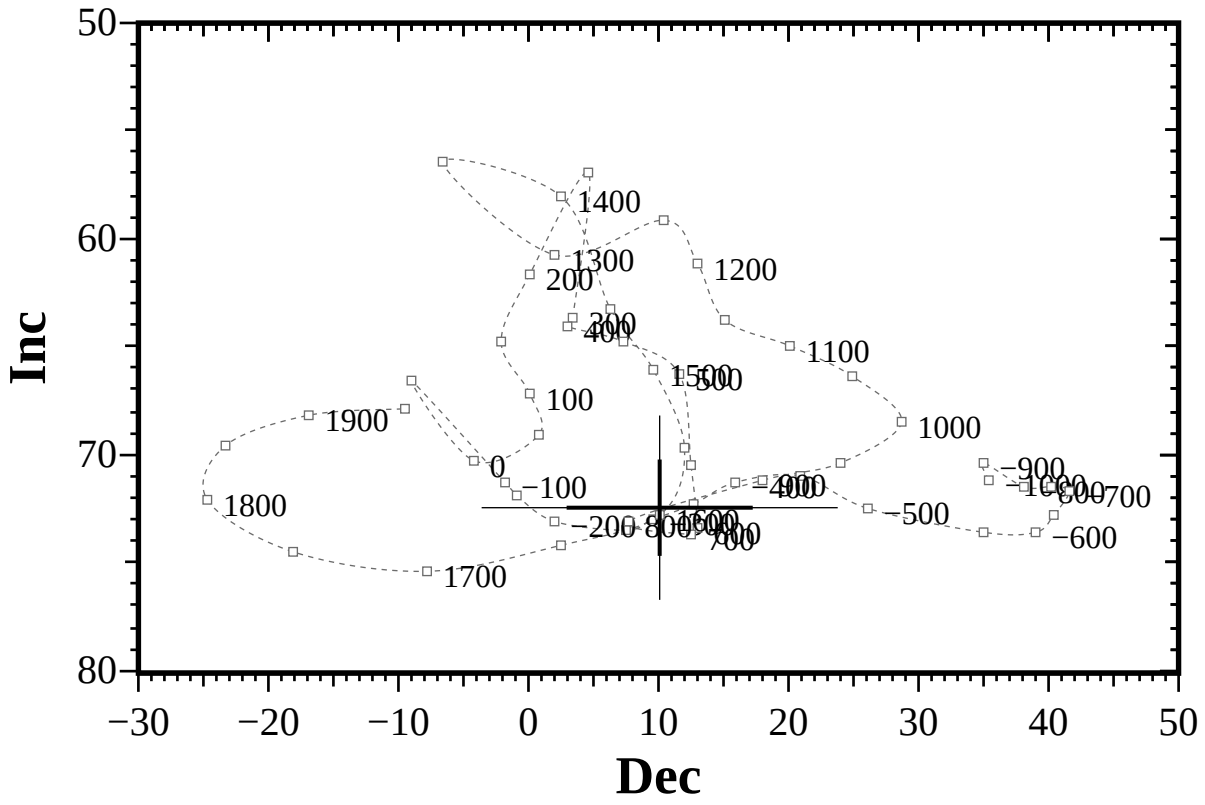

Figure 7: Comparison of the mean thermoremanent vector for context 255 calculated from samples 01, 03-06, 08-09, 14 and 16 after partial demagnetisation with the UK master calibration curve. Thick error bar lines represent 63% confidence limits and narrow lines 95% confidence limits.

a)

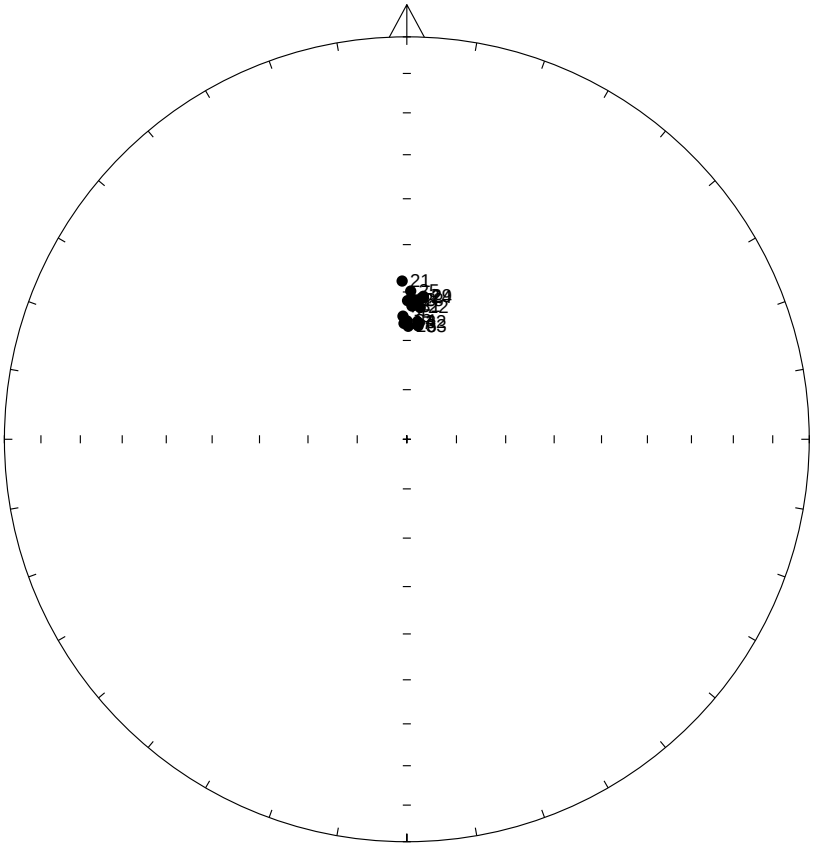

b)

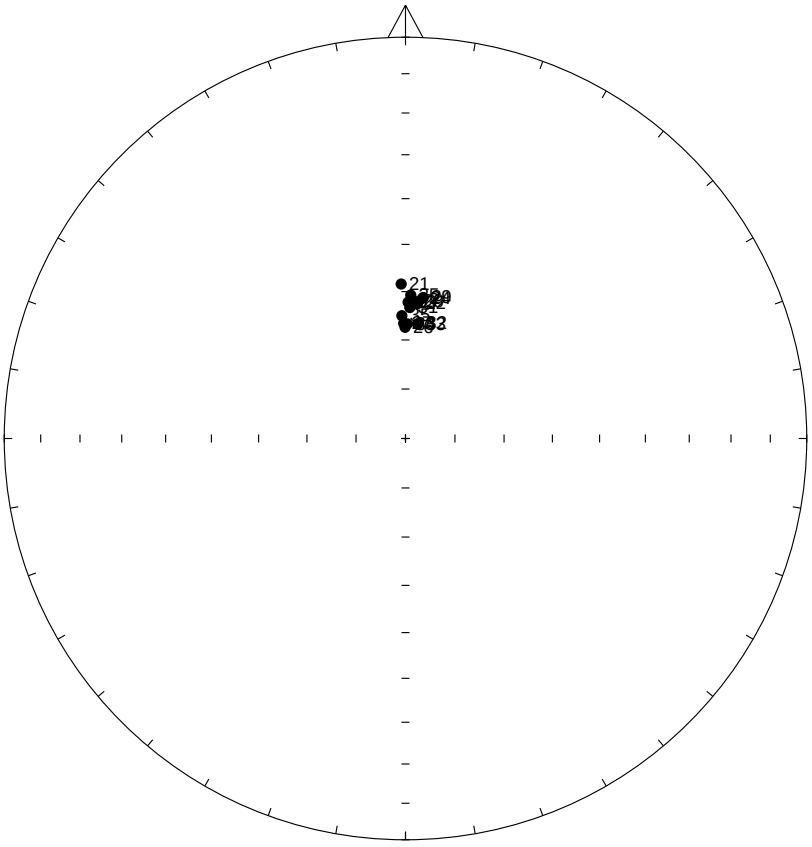

Figure 8: a) Distribution of NRM directions of samples from context 350 represented as an equal area stereogram. In this projection declination increases clockwise with zero being at 12 o'clock while inclination increases from zero at the equator to 90 degrees in the centre of the projection. Open circles represent negative inclinations. b) Distribution of thermoremanent directions of magnetisation of the same samples after partial AF demagnetisation.

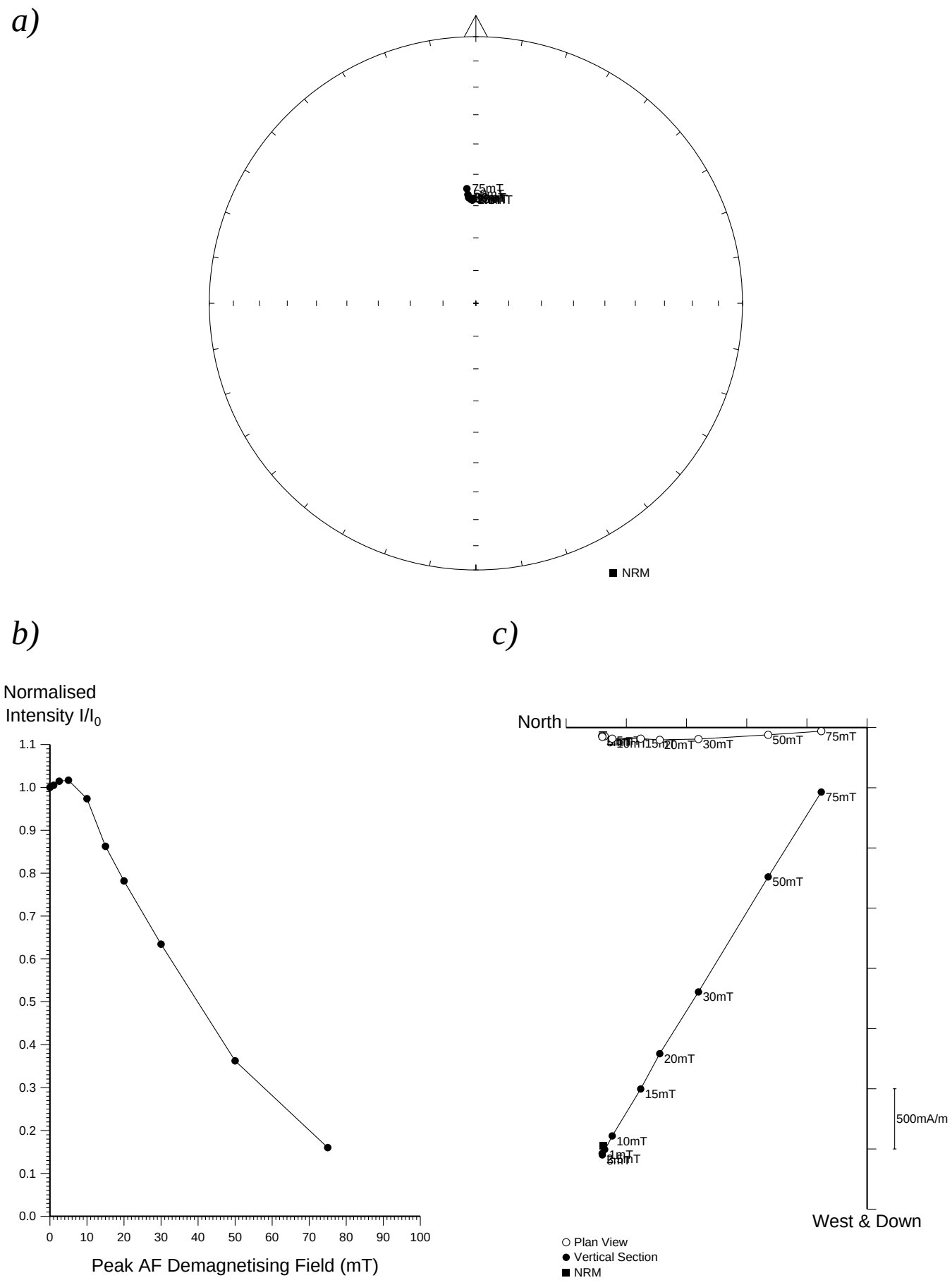

Figure 9: Stepwise AF demagnetisation of sample 21. Diagram a) depicts the variation of the remanent direction as an equal area stereogram (declination increases clockwise, while inclination increases from zero at the equator to 90 degrees at the centre of the projection); b) shows the normalised change in remanence intensity as a function of the demagnetising field; c) shows the changes in both direction and intensity as a vector endpoint projection.

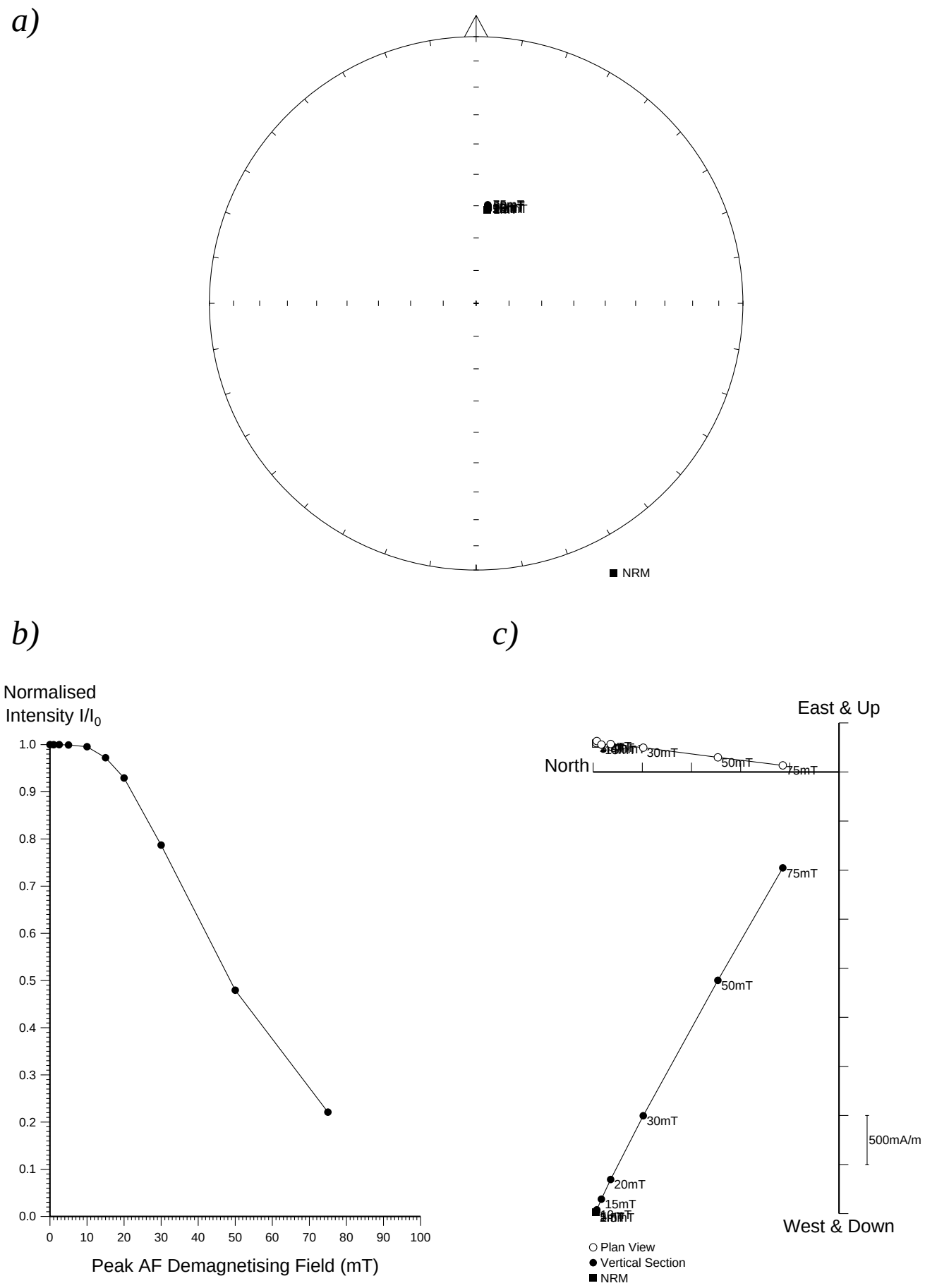

Figure 10: Stepwise AF demagnetisation of sample 24. Diagram a) depicts the variation of the remanent direction as an equal area stereogram (declination increases clockwise, while inclination increases from zero at the equator to 90 degrees at the centre of the projection); b) shows the normalised change in remanence intensity as a function of the demagnetising field; c) shows the changes in both direction and intensity as a vector endpoint projection.

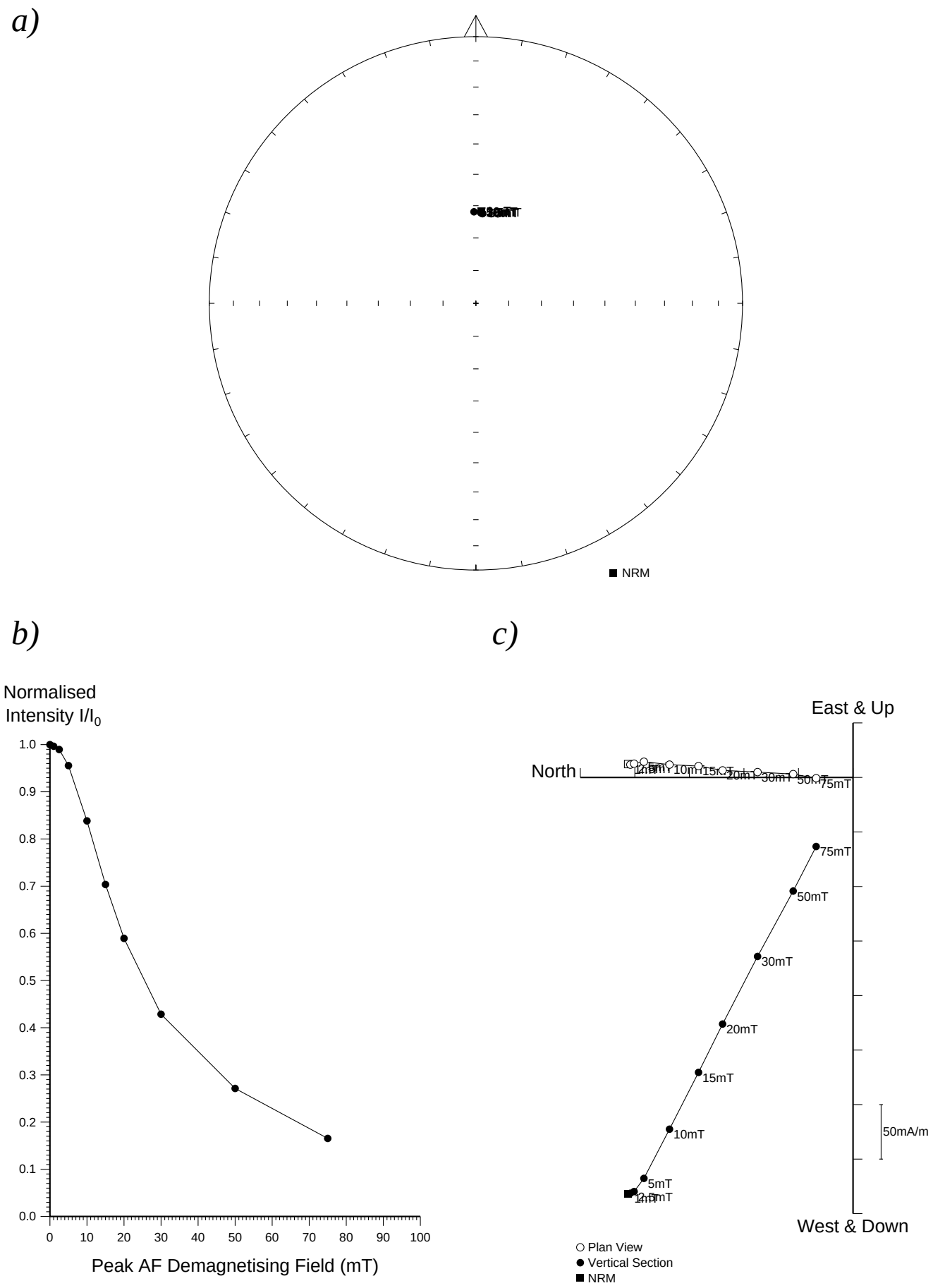

Figure 11: Stepwise AF demagnetisation of sample 28. Diagram a) depicts the variation of the remanent direction as an equal area stereogram (declination increases clockwise, while inclination increases from zero at the equator to 90 degrees at the centre of the projection); b) shows the normalised change in remanence intensity as a function of the demagnetising field; c) shows the changes in both direction and intensity as a vector endpoint projection.

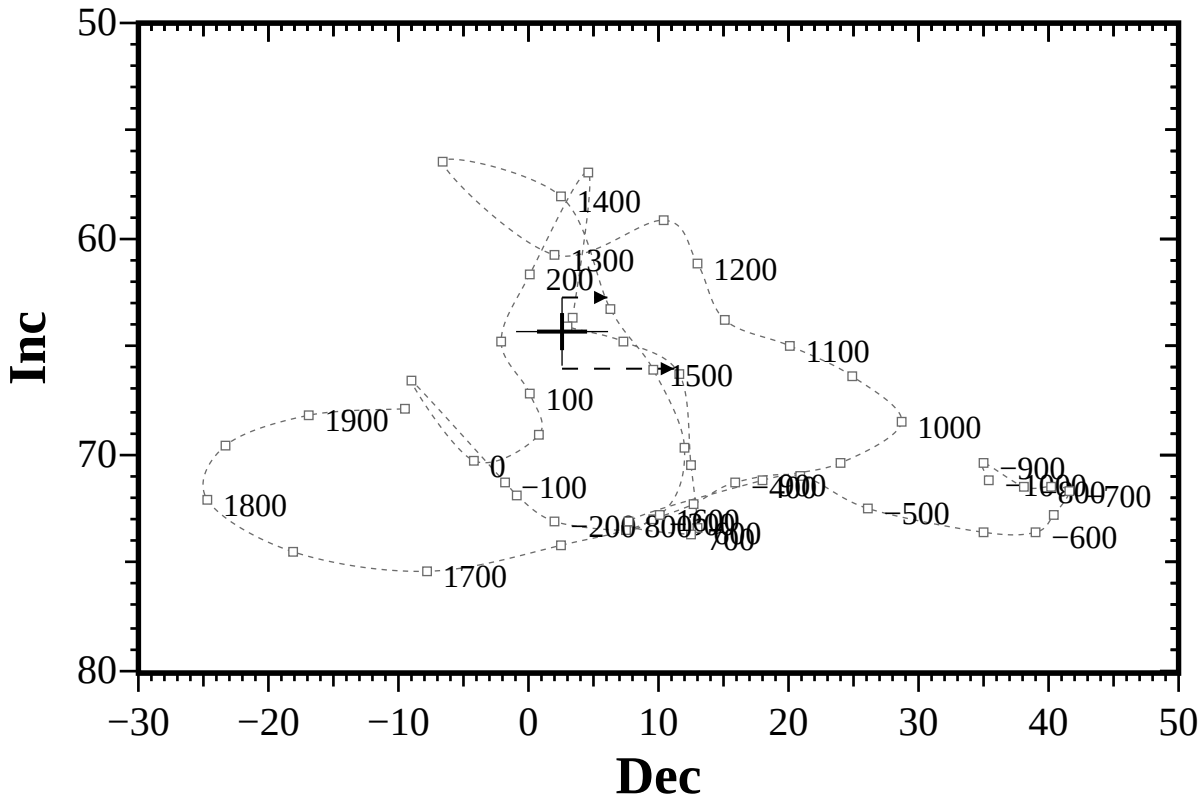

Figure 12: Comparison of the mean thermoremanent vector for context 350 calculated from samples 21-29 and 31-35 after partial demagnetisation with the UK master calibration curve. Thick error bar lines represent 63% confidence limits and narrow lines 95% confidence limits. Arrows show projection of this mean TRM direction Eastwards onto the late medieval portion of the calibration curve.